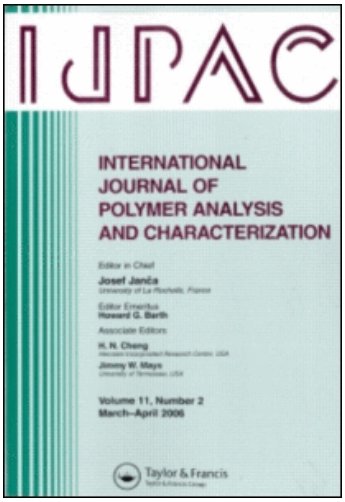

International Journal of Polymer Analysis and Characterization
Publication details, including instructions for authors and subscription information:
http://www.informaworld.com/smpp/title~content=t713646643

Nanocharacterization of Proton Radiation Damage on Magnetically Oriented Epoxy

M. S. Al-Haik[a]; S. Trinkle[a]; O. Momotyuk[b]; B. T. Roeder[b]; K. Kemper[b]; M. Y. Hussaini[c]; K. J. Malloy[d]
[a] Department of Mechanical Engineering, University of New Mexico, Albuquerque, New Mexico, USA [b] Department of Physics, Florida State University, Tallahassee, Florida, USA [c] School of Computational Science, Florida State University, Tallahassee, Florida, USA [d] Center for High Technology Materials, University of New Mexico, Albuquerque, New Mexico, USA

To cite this Article Al-Haik, M. S. , Trinkle, S. , Momotyuk, O. , Roeder, B. T. , Kemper, K. , Hussaini, M. Y. and Malloy, K. J.(2007) 'Nanocharacterization of Proton Radiation Damage on Magnetically Oriented Epoxy', International Journal of Polymer Analysis and Characterization, 12: 6, 413 — 430
To link to this Article: DOI: 10.1080/10236660701551638
URL: http://dx.doi.org/10.1080/10236660701551638

International Journal of Polymer Anal. Charact., 12: 413–430, 2007

ISSN: 1023-666X print
DOI: 10.1080/10236660701551638

Taylor & Francis
Taylor & Francis Group

Nanocharacterization of Proton Radiation Damage on Magnetically Oriented Epoxy

M. S. Al-Haik and S. Trinkle
Department of Mechanical Engineering, University of New Mexico, Albuquerque, New Mexico, USA

O. Momotyuk, B. T. Roeder, and K. Kemper
Department of Physics, Florida State University, Tallahassee, Florida, USA

M. Y. Hussaini
School of Computational Science, Florida State University, Tallahassee, Florida, USA

K. J. Malloy
Center for High Technology Materials, University of New Mexico, Albuquerque, New Mexico, USA

Abstract: In this study we investigate the shielding effectiveness of a structural epoxy against high-energy proton radiation. To study the influence of material texture on its radiation shielding effectiveness we induced orientations in the epoxy using a high magnetic field of 15 T and exposed it to proton beams of energy 6–15 MeV. The microstructure of the samples was characterized using ESEM and AFM microscopy. The effect of the radiation on the mechanical properties of the epoxy samples such as modulus and hardness was measured using nanoindentation tests.

Received 7 May 2007; accepted 1 July 2007.
We acknowledge the support of the State of Florida, the National Science Foundation (NSF), and the National High Magnetic Field Laboratory (NHMFL), Tallahassee, Florida for making this work possible.
Address correspondence to M. S. Al-Haik, Department of Mechanical Engineering, University of New Mexico, Albuquerque, NM 87131, USA. E-mail: alhaik@unm.edu

Keywords: Epoxy; Magnetic alignment; Nanoindentation; Proton irradiation

INTRODUCTION

Radiation in space affecting human operations stems from three types of charged particles, electrons, protons, and all the known chemical elements up to Ni over a broad energy spectrum with significant fluence in the range of 0.1 to 10 GeV/nucleon.[1] The three sources of radiation are (i) particles of galactic origin (galactic cosmic rays), (ii) particles engendered by the acceleration of solar plasma due to strong electromotive forces in the solar surface and the acceleration across the transition shock boundary of propagating coronal mass ejecta (solar energetic particles), and (iii) particles trapped within the confines of the geomagnetic field. The trapped radiation mainly comprises protons and electrons within two bands centered on the geomagnetic equator reaching maximum intensity at an altitude of 3600 km, followed by a minimum at 7000 km and a second very broad maximum at 10000 km.[2] In passing through shield materials, the heavy ions lose kinetic energy by transfer to orbital electrons. Since galactic cosmic ray (GCR) ions are of high energy, they may be fragmented into nuclear remnants, generating new particles by colliding with the nuclei in the shield. As a consequence, GCR ions and their reaction products continue to penetrate the shield material and expose the astronaut to radiation.[3] Solar particle events (SPE) are sporadic and have lower energies, and they mainly consist of protons and helium ions, with energies usually less than 1.0 GeV/nucleon.[1] SPEs have always been a primary concern for operations outside the Earth's protective magnetic field, as they could deliver potentially lethal exposures over the course of several hours.[4] The trapped radiation has constrained human Earth orbital operations to altitudes below 3600 km, beyond which potentially lethal exposures are obtained over tens of hours.[2]

In 1989, the National Council on Radiation Protection[5] estimated that only 2.5 g/cm^2 of aluminum would be required to meet the 500 mSv limit (the limit is now 200 mSv) for the exposure of blood-forming organs. This limit is strictly for low earth orbit (LEO), but if it is used as a guideline, it is estimated that the Mars Reference Mission will require an aluminum shield thickness above 50 g/cm^2, which is obviously impractical.[1] Several materials have been identified as potentially important for future shields. These are liquid hydrogen, hydrogenated nanofibers, liquid methane, LiH, polyethylene, polysulfone, and polyetherimide (in order of improving shield performance).[6]

A material that can adsorb the energy of cosmic radiation without cascading is a necessity for deep-space radiation shielding. Tests at

NASA Langley Research Center have verified that liquid hydrogen with minimal cascading effect is the best shield of cosmic radiation.[6] Therefore, a better shield against space radiation will comprise a material that has a lot of hydrogen, yet is solid and can withstand the traditionally stringent requirements of space travel. Polymers have high hydrogen content, and in a crystalline state (e.g., polyethylene), they have a very predictable uniform concentration throughout the shield. They also comprise carbon and oxygen, which are lightweight elements with negligible cascading properties. Polymeric substances exhibit a wide variety of radiation effects. The formation of new chemical bonds after irradiation usually results in irreversible effects. Generally, these are manifested as changes in appearance, chemical and physical states, and mechanical, electrical, and thermal properties.[7]

In general, the exposure of polymers to ionizing radiation will alter their basic molecular structure and associated macroscopic properties. These molecular changes are brought about through a complex set of reactions upon exposure to radiation energy. Polymers are altered primarily through two basic schemes: charge absorption and subsequent cleavage that give rise to radical formation, radical combination resulting in the formation of cross-links, or disproportionation to give scission, and gas evolution.[8]

In general, for flexible polymers that experience cross-linking as a result of ionization, the elastic modulus tends to increase while the strain to failure decreases. Chain scission results in a decrease in Young's modulus, reduced yield stress for plastic flow, increased elongation, decreased hardness, and decreased elasticity. It sometimes causes embrittlement and release of gas. Gao et al.[9] performed irradiation of 160 keV protons for AG-80 epoxy resin and examined changes in bend strength, bend modulus, interlayer shear strength, and mass loss ratio. Experimental results showed that increasing proton fluence lowered the cross-linking density as well as the bend strength, and bend modulus decreased.

Parada et al.[10] bombarded two polymers, tetrafluoroethylene-per-fluoromethoxyethylene (PFA) and tetrafluoroethylene-hexa-fluoropropylene (FEP), with 1 MeV protons at constant current and fluence. Utilizing micro-Raman and Fourier transform-infrared measurements, the authors concluded that film damage due to proton bombardment is mainly attributed to broken C–C bonds in the polymer structures. Kudoh et al.[11] investigated changes in the mechanical properties of poly (methyl methacrylate) (PMMA) and glass fiber reinforced plastic (GFRP) induced by high energy (30, 45 MeV) protons. The flexural strength at break of PMMA and GFRP showed the same degradation behavior as a function of dose absorption.

One technique to reduce the radiation damage of an epoxy is to "tailor" its microstructure to improve its mechanical properties before

it is exposed to radiation. The ability to impose local organization of polymer materials through the rational design of chemical structure and processing methods is of continuing scientific and technological interest. Bulk orientation for polymers was shown to occur via extensional shear obtained by melt spinning[12] and injection molding.[13] Magnetic field induced alignment of polymeric materials has been the focus of several research efforts.[14–17] Polymers can interact with a magnetic field through the diamagnetic anisotropy of its constituent repeating units. The energy that the repeating unit gains through the interaction with an external magnetic field is dependent on the orientation of the unit relative to the magnetic field, and hence the unit tends to align in a certain direction that optimizes energy reduction.[18] If the energy reduction is insufficient compared to its thermal energy, the tendency of a unit to align is suppressed by molecular vibrations. The application of a magnetic field during polymer processing may achieve enhanced mechanical and physical properties compared to mechanical stretching. For example, a magnetic field was applied during the cure reaction of a liquid crystalline epoxy,[19, 20] resulting in alignment of the molecules along the direction of the applied field. The orientation parameters attained a maximum level at a field strength of approximately 12 tesla. The elastic tensile modulus increased with the square of the orientation parameter, attaining a maximum value of 8.1 GPa, compared to 3.1 GPa for the non-oriented material. The authors utilized high magnetic fields to reorient commercial epoxy (15–25 tesla). Reported improvements included mechanical properties (Young's modulus, universal hardness) and physical properties (thermal and electrical conductivities).[21–23]

The purpose of the current work is to investigate both the shielding effectiveness and the mechanical-property degradation of a structural epoxy exposed to intense proton beams and also to explore the effect of magnetic processing on the mechanical properties and shielding effectiveness.

EXPERIMENTAL SECTION

Materials

Aeropoxy was used as the matrix. It is a medium-viscosity, unfilled, light amber laminating resin designed for structural production applications. According to the specifications furnished by the manufacturer (PTM&W Industries, Inc., Santa Fe Springs, Calif., USA), the components of the epoxy used here are Aeropoxy PR2032, a material containing diphenylolpropane (bisphenol A), and a multifunctional acrylate; the hardener component Aeropoxy PH3660 is a modified amine mixture. The epoxy

Table I. Physical and mechanical properties of the epoxy system

Property	PH2032 (Epoxy resin base)	PH3660 (Curing agent)
Viscosity	90 N s/m2	95 N s/m2
Mix ratio by weight	100	27
Density of the mix	1.11 kg/L	
Glass-transition temperature	91°C	
Pot life (4 oz)	50–60 min	
Tensile strength	67.8 MPa	
Tensile modulus	2.89 GPa	

also contains some acrylic monomers. These materials do not contain metallic compounds of any kind. The absence of metallic compounds in the epoxy resin eliminates the possibility of metallic compound induced orientation of the polymer bundles, and this attributes the response to the magnetic field to the polymer network itself. This resin laminates very easily and wets out fiberglass, carbon, and Kevlar Aramid fibers readily. Used with the PH3660 hardener, this system cures at room temperature for 24 h. The typical properties of this epoxy are listed in Table I.

The components were mixed mechanically by sonication for 10 min. The mix ratio for each sample was 4:1 (w/w). The epoxy system was degassed moderately until no gas bubbles could be seen, and then it was injected inside a square cross section plastic tube with dimensions of 10 mm × 10 mm × 50 mm. The tubes were sealed and wrapped around a sample holder with nonmagnetic tape.

Magnetic Processing

The magnetic processing of the samples was carried out at the National High Magnetic Field Laboratory (NHMFL), Tallahassee, Florida. The magnetic fields were generated in a 20 tesla direct-current (DC) resistive solenoid. This magnet had a large bore (190 mm) so it could accommodate a furnace. The temperature in the furnace was provided by a heating element and was measured by a Pt thermocouple, which had low magnetic properties. A proportional-integral derivative (PID) controller controlled the temperature. Once the sample holder was placed inside the furnace, the furnace was pushed into the magnet bore so that the samples were in the center of the magnetic field, and the magnet was subsequently brought up to a 15 T field. The samples were left to cure at room temperature inside the field for 2 h with no applied heat so that the viscosity

remained as low as possible. Then, the furnace was heated to 60°C, and the samples were left to cure under the magnetic field for another 2 h. Subsequently, the magnetic field was reduced to 0 tesla, and the samples were placed in another furnace at 60°C for another 2 h to ensure full cure.

Proton Radiation

The Florida State University tandem Van de Graaff accelerator was used to provide energetic beams of protons. The tandem Van de Graaff accelerator can be used as a stand-alone accelerator, or it can inject a superconducting linear accelerator that can boost the beam energy further. The accelerators are capable of producing proton beams for experiments with continuously variable energies from 2 to 20 MeV and beams of all other nuclear species up to mass 40 except for the noble gases Ne and Ar, with energies up to 6 MeV per amu for the beams over mass 28 and up to 8 MeV per amu for lighter beams.

The experimental setup for the energy loss measurement is shown in Figure 1. Collimating slits and apertures were used to limit the size and angular divergence of the incident beam. The direct beam from the accelerator is much more intense than desired for the work here. Consequently, the direct beam struck a thin gold foil, and the scattered protons from this foil irradiated the samples of interest. The experiment was conducted in a vacuum scattering chamber. The scattered protons were detected in a Si surface barrier detector that was calibrated so that the proton energy could be read out directly. The energy loss of protons

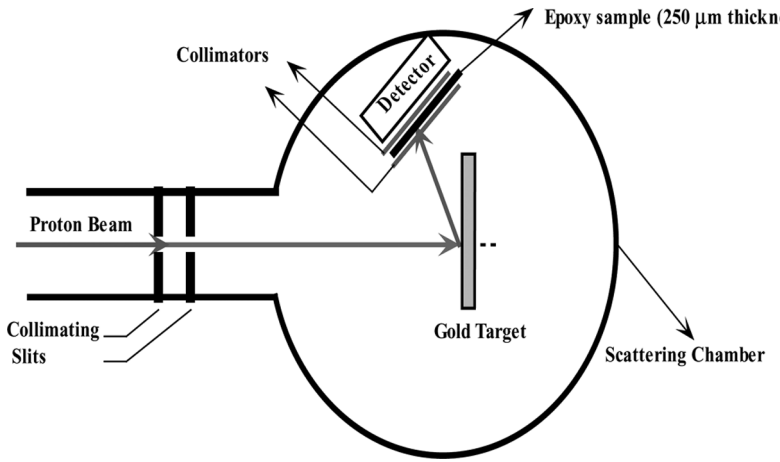

Figure 1. Schematic diagram showing relative positions of target and detectors.

passing through the sample was found by determining the energy difference between protons with and without the sample being placed in front of the detector. Each sample was exposed to five different initial beam energies between 6 and 15 MeV for 10 min at each energy level.

RESULTS AND DISCUSSION

The estimated uncertainty in experimental stopping power value is approximately 2.5%, as derived from a conservatively estimated average statistical uncertainty. The shielding effectiveness was measured in terms of the number of high-energy particles in the beam before and after it impinges on the epoxy film.

Following the steps proposed by Ammi et al.[24] and Trzaska et al.,[25] the stopping power in the sample was determined by dividing the energy loss by the sample areal density.

The comparison of the stopping powers of the different epoxy samples is shown in Figure 2. The magnetically processed samples have shown less stopping power than those processed outside the magnetic field.

Charged particles of a given initial energy have a maximum distance or range they can travel through a medium before they are stopped and become incorporated into the medium. A charged particle is slowed to a

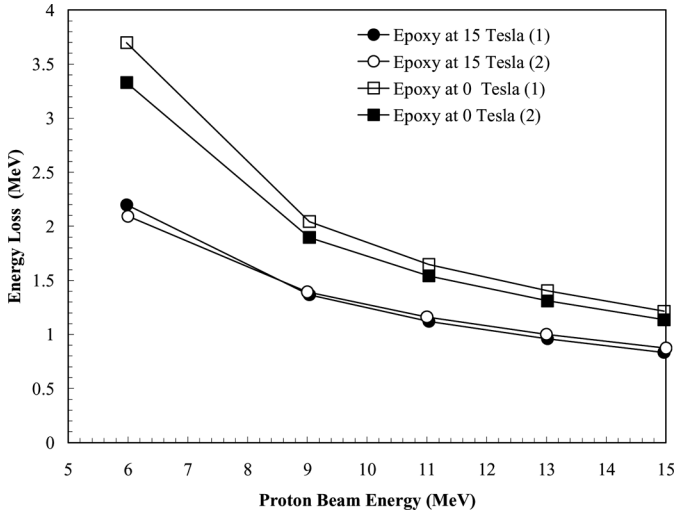

Figure 2. Energy loss plots for four different epoxy samples. Proton beams were applied progressively to the samples between 6 and 15 MeV.

lower kinetic energy after traveling a distance along its path, as a result of both coulombic interactions with (atomic) electrons and finally nuclear stopping at the end of its path.[26] Heavy charged particles (those with masses greater than or equal to the proton mass), with kinetic energies much less than their rest-mass energies, slow down almost entirely due to coulombic interactions. A multitude of such interactions take place—so many that the slowing down is virtually continuous and along a straight-line path. These interactions, taken individually, may range from ionization processes producing energetic recoil electrons (delta rays) to weak atomic or molecular excitation that may not result in ionization at all. The magnetic alignment will introduce shorter channels for protons to travel and therefore will not slow the protons as much as a randomly organized epoxy.

Microscopy

The microstructures of two samples, one cured without the magnetic field and the other magnetically processed under a 15 tesla field, were examined. Sample surfaces, pre-radiation and post-radiation, were examined using an Electroscan model E-3 environmental scanning electron microscopy (ESEM) facility.

The appearance before and after proton-beam bombardment is shown in the ESEM micrographs of Figure 3. The surface of the sample processed without the magnetic field shows no preferred orientation (Figure 3(A)). Initially, the surface of the epoxy sample is smooth with no distinct features. The application of a 15 tesla magnetic field leads to the development of domains within which the chains of the epoxy polymer are oriented in the direction of the field. The magnetically developed morphology of the epoxy takes a fibril shape (Figure 3(B)). The optical orientation of the domains appears to be relatively uniform. Upon irradiation, the samples processed outside the field suffered significant damage, as shown in Figure 3(C). After bombardment the surface became rough due to the uneven loss of mass. After bombardment, the sample processed under the 15 tesla field (Figure 3(D)) maintained the fibril microstructure with less defined boundaries, but the intensity of the fibrils decreased and the surface color became much darker, an indication of oxidation.

Morphology of the epoxy specimen surface was observed using a Digital Instruments CP-II (CP-II) scanning probe microscope/atomic force microscope (SPM)/(AFM). The AFM is equipped with a Veeco silicon tip oscillating slightly below its resonance frequency (300 kHz). The samples processed under the 15 T magnetic field show less damage than the samples that were not magnetically annealed. As evident by the

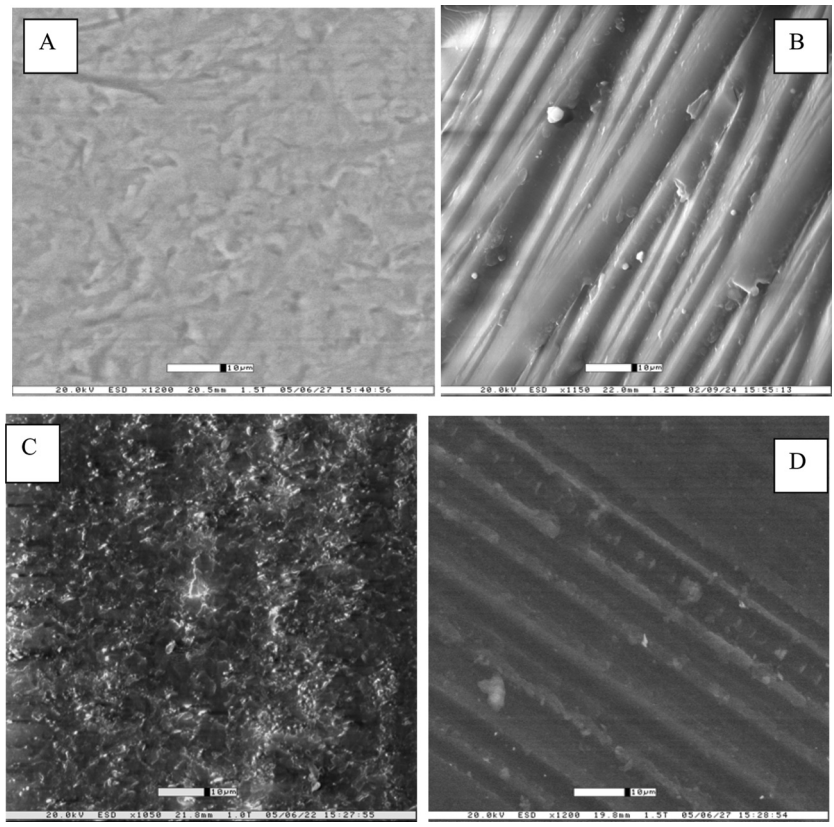

Figure 3. (A) ESEM micrograph of sample processed at 0 T; (B) ESEM micrograph of sample processed under 15 T; (C) sample in (A) after proton irradiation; (D) sample in (B) after proton irradiation. Scale bar is 10 μ.

AFM scans, shown in Figure 4, the surface of the magnetically annealed samples after irradiation is smoother than that of the samples processed with no magnetic field. This increase in roughness is an indication that the surface suffered plastic deformation.

Nanoindentation

Continuous depth sensing indentation provides load-displacement plots, which act as a mechanical fingerprint. Nanoindentation was carried out using a NanoTest 600 (Micro Materials, Wrexham, UK). A schematic diagram of the instrument is shown in Figure 5. A diamond Berkovich indenter is attached to a pendulum that moves freely around an

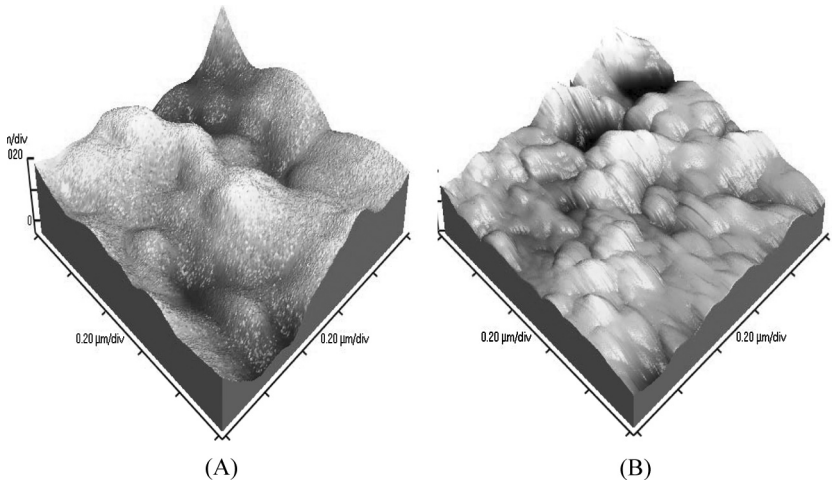

Figure 4. AFM scans of irradiated samples; (A) samples processed under 0 T, (B) sample processed under 15 T.

essentially frictionless pivot. The indenter is loaded against the sample by passing a current through the coil, which is then drawn to the permanent magnet. Displacement of the indenter into the sample is measured by the variation in voltage between the capacitance plates. The sample holder is aligned with the indenter by means of three DC motors that run XYZ micrometer stages. This arrangement is mounted on a separate stage and allows movement between the indenter and a high-resolution zoom microscope. The zoom microscope allows high precision selection of areas for indentation.

Nanoindentations were carried out at load level of 5 mN for all the materials tested to enable a comparison of mechanical properties. The loading rate was set to 0.25 mN/s. A minimum distance of 5 µm was set between each indentation. For each sample, 25 nanoindentation tests were carried out to calculate both the hardness and modulus values. Figure 6 shows two hysteresis series for a sample that was indented pre- and post-bombardment.

The hold time at maximum load was designed to allow for the sample to "creep out" before unloading. The second hold period (after unloading to a low load level) was carried out to account for thermal drift. For samples that are susceptible to creep (e.g., metals and polymers) 30 s hold periods may be needed, according to NanoTest developers.[27]

The main properties of interest are Young's modulus and hardness. There are a number of methods available to analyze load-displacement curves; the technique employed in this study is that developed by Oliver

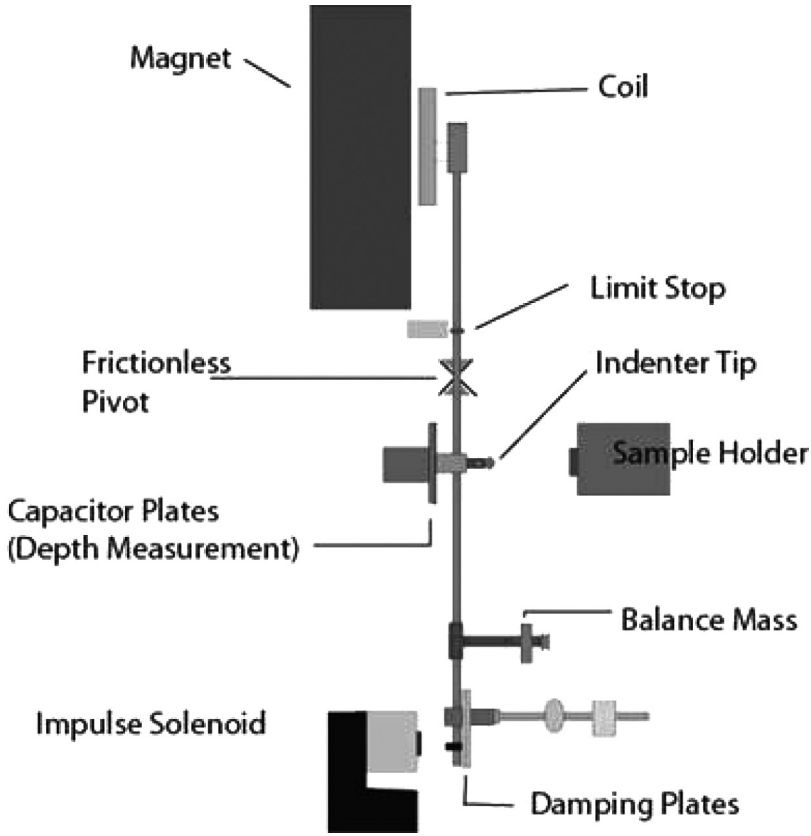

Figure 5. Schematic diagram of the NanoTest system.

and Pharr.[28] The calculation of hardness and Young's modulus from indentation experiments requires the following information: peak load (P_{max}), maximum depth (h_{max}), contact compliance (C) at initial stage of unloading, and a geometric function A (h_c) related to the indenter geometry.

The depth versus loading-unloading data for each indentation curve, shown in Figure 6, was fitted to a power function to determine the mechanical properties of the test sample. The power law function has the form:

$$P = a(h - h_c)^m \tag{1}$$

where a, h_c, and m are constants. The plastic depth, h_c, is critical for determining the diamond projected area for modulus and hardness

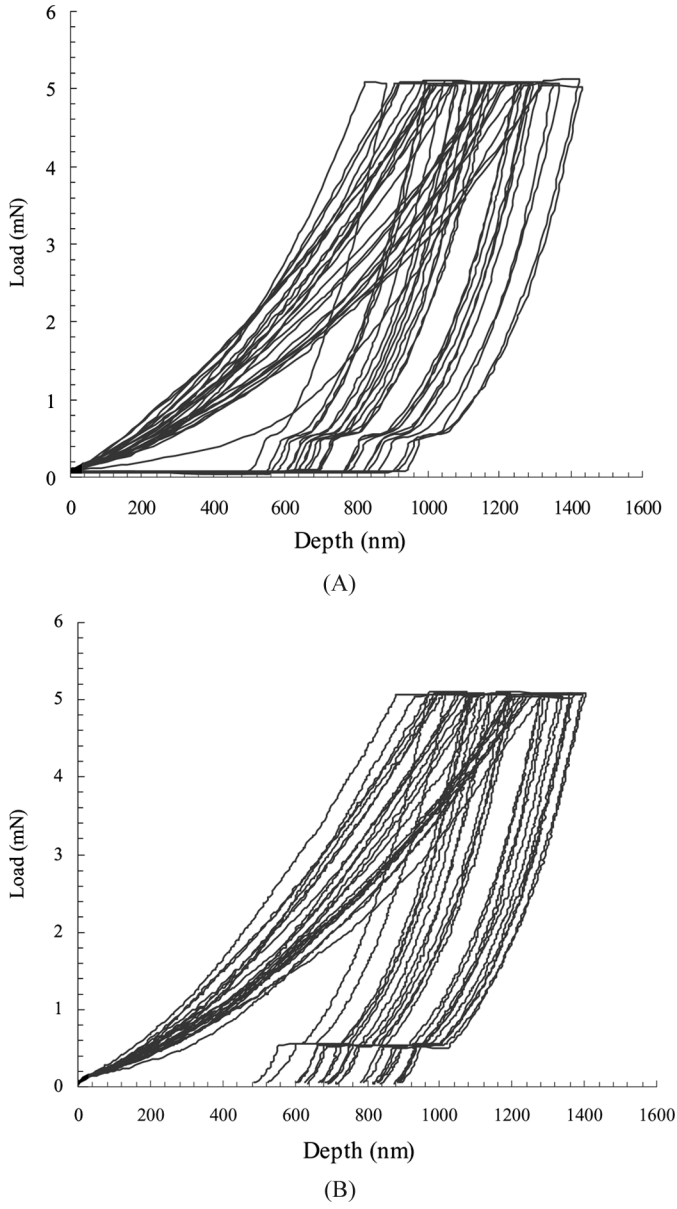

Figure 6. Nanoindentation curves for 25 different loading-unloading cycles at a maximum load of 5 mN; (A) sample processed outside the field pre-radiation, (B) sample processed outside the field post-radiation.

calculation and is determined from the expression:

$$h_c = h_{\max} - e(CP_{\max}) \tag{2}$$

where C is the contact compliance equal to the tangent at maximum load. The value of e depends on the indenter geometry. For a Berkovich indenter, e is 0.75. The diamond area function a (h_c) has been previously determined, according to the calibration of a fused silica sample as shown in Figure 7.

The hardness (H) is determined from the peak load ($P_{\max}$) and the projected area of contact, A:

$$H = \frac{P_{\max}}{A} \tag{3}$$

To obtain the elastic modulus, the unloading portion of the depth-load curve is analyzed according to a relation that depends on the contact area:

$$C = \frac{\sqrt{\pi}}{2E_r\sqrt{A}} \tag{4}$$

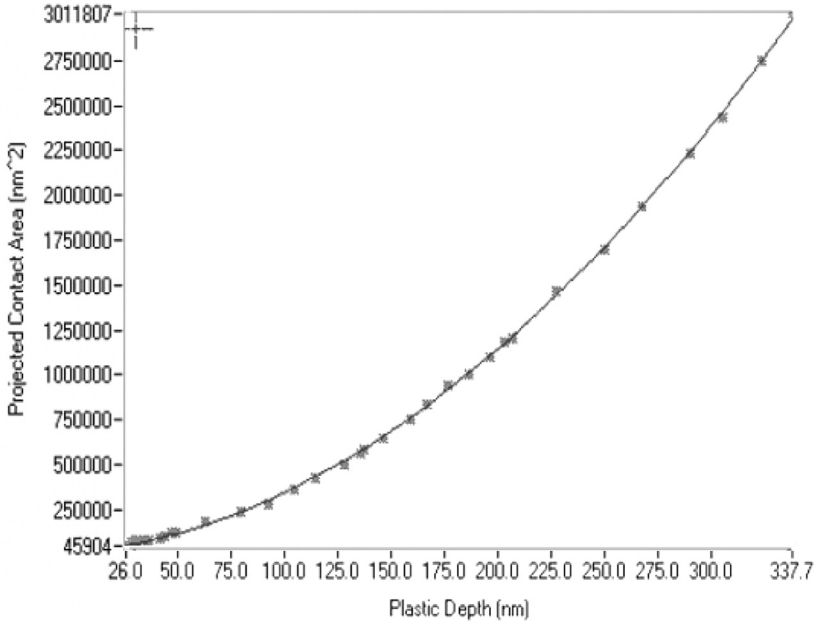

Figure 7. Diamond area function plot obtained from calibration sample.

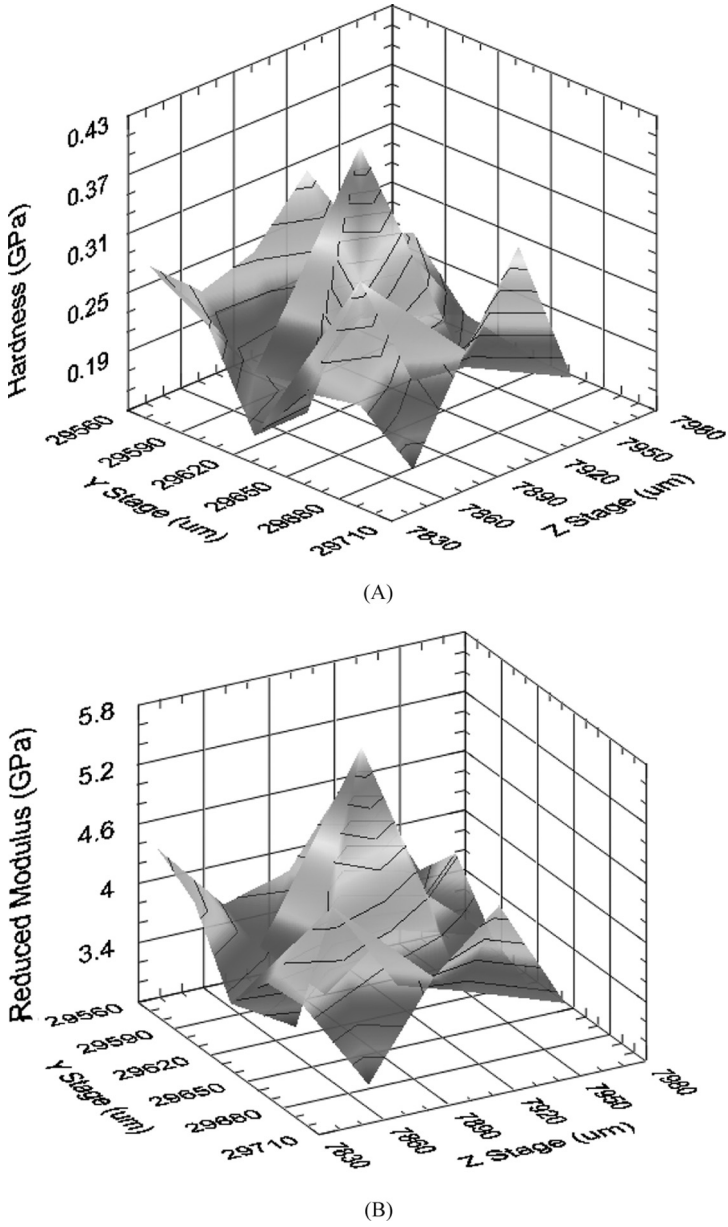

Figure 8. (A) Hardness and (B) reduced modulus variation maps for a sample processed outside the magnetic field before proton bombardment. Each property was measured at 25 different locations within the sample surface.

where C is the contact compliance and E_r is the reduced modulus defined by

$$\frac{1}{E_r} = \frac{(1 - n_s^2)}{E_s} + \frac{(1 - n_i^2)}{E_i} \tag{5}$$

where n_s = Poisson's ratio for the sample, n_i = Poisson's ratio for the indenter (0.07), E_s = Young's modulus for the sample, and E_i = Young modulus for the indenter (1141 GPa).

Application of the load to the indenter and the resulting displacement represent work done on the system and are manifested as both plastic and elastic strains within the specimen. The net area enclosed by the load-displacement response represents the energy lost in plastic deformation within the specimen. This plastic work is indicative of the sample toughness.[29]

Variations of the modulus and hardness properties over 25 indentations are shown in Figure 8. These maps were generated from analyzing nanoindentation results for a sample that was neither magnetically annealed nor bombarded with protons. The values of hardness, modulus, and plastic work for each sample are shown in Table II. These values are averaged over 25 indentation tests per sample. It is apparent from Table II that the magnetically induced texture enhanced the hardness and modulus but decreased the plastic work along the orientation of the magnetic field. The magnetically annealed sample showed an increase of 19.2% in terms of the modulus and 38.2% for the hardness compared to the sample processed outside the magnetic field. The magnetic processing, however, made the sample more brittle, as the plastic work reduced by 8.3%. Bombarding the samples with proton beams degraded both the modulus and toughness (plastic work) but increased the hardness. The degradation percentage in mechanical properties due to radiation was significant for both samples. However, the post-radiation magnetically annealed sample maintained higher modulus and hardness values than the other sample but showed less toughness.

Table II. Mechanical properties of samples pre- and post-bombardment with series of proton beams 6–15 MeV

Sample	Hardness (GPa)	Modulus (GPa)	Plastic work (nJ)
0 T, no radiation	0.1918 ± 0.016	3.4714 ± 0.246	1.92 ± 0.321
0 T, irradiated	0.2387 ± 0.062	2.3820 ± 0.410	1.80 ± 0.158
15 T, no radiation	0.2652 ± 0.035	4.1375 ± 0.312	1.76 ± 0.258
15 T, irradiated	0.2973 ± 0.047	2.8822 ± 0.200	1.70 ± 0.2871

CONCLUSIONS

Magnetic processing significantly affects the mechanical behavior of the epoxy system; it becomes stiffer, harder, and more brittle than samples processed without magnetic fields. The application of a 15 tesla magnetic field leads to the development of domains within which the chains of the epoxy polymer are oriented in the direction of the field. The magnetically developed morphology of the epoxy takes a fibril shape. The magnetically induced texture reduces the stopping power of protons compared to those samples processed without the magnetic field. However, the magnetically processed epoxy shows less degradation in modulus and hardness post-radiation with successive proton beams. Therefore, there is a trade-off between shielding effectiveness and mechanical properties of the epoxy. The results of this investigation can be utilized to determine efficient shield thicknesses necessary to attenuate (or stop) the protons before they can cause biological damage. Using thicker samples, more than 250 μm, will yield more proton energy loss (better shielding). Hence, by utilizing magnetic processing, a multifunctional epoxy with "optimal" microstructure can be "tailored" toward both radiation shielding and structural applications.

REFERENCES

[1] Wilson, J. W., F. A. Cucinotta, J. Miller, J. L. Shinn, S. A. Thibeault, R. C. Singleterry, L. C. Simonsen, and M. H. Kim. (2001). Approach and issues relating to shield material design to protect astronauts from space radiation. *Mater. Des.* **22**(7), 541–554.

[2] Stassenopolous, E. G. (1986). In *High-Energy Radiation Background in Space: CHERBS—1987, Sanibel Island, Florida*, eds. A. C. Rester, Jr. and J. I. Trombka. New York: American Institute of Physics, p. 3.

[3] Wilson, J. W., J. L. Shinn, R. K. Tripathi, R. C. Singleterry, and M. S. Clowdsley. (2001). Issues in deep space radiation protection. *Acta Astronaut.* **49**(3–10), 289–312.

[4] Wilson, J. W. and F. M. Denn. (1976). *Preliminary Analysis of the Implications of Natural Radiations on Geostationary Operations*. NASA TN D-8290. Langley, Va.: Langley Research Center.

[5] National Council on Radiation Protection and Measurements. (1989). *Guidance on Radiation Received in Space Activities*. NCRP Report No. 98. Bethesda, Md.: NCRP.

[6] Wilson, J. W., J. Miller, A. Konradi, and F. A. Cucinotta. (1997). *Shielding Strategies for Human Space Exploration*. NASA Publication 3360.

[7] NASA Space Vehicle Design Group. (1970). *Nuclear and Space Radiation Effects on Materials—Space Vehicle Design Criteria*. NASA SP-8053.

[8] Chapiro, A. (1962). *Radiation Chemistry of Polymeric Systems*. New York: Wiley Interscience.

[9] Gao, Y., S. Jiang, D. Yang, S. He, J. Xiao, and Z. Li. (2005). A study on radiation effect of 200 keV protons on M40J/epoxy composites. *Nucl. Instrum. Methods Phys. Res. Sect. B.* **229**, 261–268.
[10] Parada, M. A., A. de Almeida, C. Muntele, I. Muntele, and D. Ila. (2005). Effects of MeV proton bombardment in thin film PFA and FEP polymers. *Surf. Coat. Technol.* **196**, 378–382.
[11] Kudoh, H., T. Sasuga, T. Seguchi, and Y. Katsumura. (1996). High energy ion irradiation effects on polymer materials: 2. Proton irradiation effects on PMMA and GFRP. *Polymer* **37**(21), 4663–4665.
[12] Yuan, X., A. F. T. Mak, K. W. Kwok, B. Yung, and K. Yao. (2001). Characterization of poly (L-lactic acid) fibers produced by melt spinning. *J. Appl. Polym. Sci.* **81**(1), 251–260.
[13] Kalay, G. and M. J. Bevi. (1997). The effect of shear controlled orientation in injection molding on the mechanical properties of an aliphatic polyketone. *J. Polym. Sci. Part B Polym. Phys.* **35**(3), 415–430.
[14] Kimura, T., T. Kawi, and Y. Sakamoto. (2000). Magnetic orientation of poly (ethylene terephthalate). *Polymer* **41**(2), 809–812.
[15] Kawai, T., Y. Sakamoto, and T. Kimura. (2000). Melt structure of crystalline polymers as studied by means of magnetic orientation. *Mater. Trans. JIM* **41**(8), 955–961.
[16] Anwer, A. and A. H. Windle. (1993). Magnetic orientation and microstructure of main-chain thermotropic copolyesters. *Polymer* **34**(16), 3347–3357.
[17] Kimura, T., M. Yamato, W. Koshimizu, M. Koike, and T. Kawai. (2000). Magnetic orientation of polymer fibers in suspension. *Langmuir* **16**(2), 858–861.
[18] Kossikhina, S., T. Kimura, E. Ito, and M. Kawahara. (1997). Structures and tensile properties of a magnetically and mechanically oriented liquid crystalline copolyester, Xydar. *Polym. Eng. Sci.* **37**(2), 396–403.
[19] Lincoln, D. M. and E. P. Douglas. (1999). Control of orientation in liquid crystalline epoxies via magnetic field processing. *Polym. Eng. Sci.* **39**(10), 1903–1912.
[20] Benicewicz, B. C., M. E. Smith, J. D. Earls, Jr., R. D. Priester, S. M. Setz, R. S. Duran, and E. P. Douglas. (1998). Magnetic field orientation of liquid crystalline epoxy thermosets. *Macromolecules* **31**(15), 4730–4738.
[21] Al-Haik, M. S., H. Garmestani, D. S. Li, M. Y. Hussaini, S. S. Sablin, R. Tannenbaum, and K. Dahmen. (2004). Mechanical properties of magnetically oriented epoxy. *J. Polym. Sci. Part B Polym. Phys.* **42**(9), 1586–1600.
[22] Garmestani, H., M. S. Al-Haik, K. Dahmen, R. Tannenbaum, D. S. Li, S. S. Sablin, and M. Y. Hussaini. (2003). Epoxy mediated alignment of single wall carbon nanotubes under high magnetic fields. *Adv. Mater.* **15**(22), 1918–1921.
[23] Choi, E. S., J. S. Brooks, D. L. Eaton, M. S. Al-Haik, M. Y. Hussaini, H. Garmestani, D. Li, and K. Dahmen. 2003. Enhancement of thermal and electrical properties of carbon nanotube polymer composites by magnetic field processing. *J. Appl. Phys.* **94**(9), 6034–6039.

[24] Ammi, H., M. Chekirine, and A. Adjerad. (1997). Stopping power of 1.0–2.6 MeV protons in mylar, makrofol and cellulose nitrate foils. *Radiat. Meas.* **28**(1–6), 15–18.
[25] Trzaska, W. H., T. Alanko, V. Lyapin, and J. Raisanen. (2001). A novel method for obtaining continuous stopping power curves. *Nucl. Instrum. Methods Phys. Res. Sect. B.* **183**, 203–211.
[26] Shultis, J. K. and R. E. Faw. (2002). *Fundamentals of Nuclear Science and Engineering*. New York: Marcel Dekker.
[27] Beake, B. D., S. Chen, J. B. Hull, and F. Gao. (2002). Nanoindentation behavior of clay/poly (ethylene oxide) nanocomposites. *J. Nanosci. Nanotechnol.* **2**(1), 73–79.
[28] Oliver, W. C. and G. M. Pharr. (1992). An improved technique for determining hardness and elastic modulus using load and displacement sensing indentation experiments. *J. Mater. Res.* **7**(6), 1564–1583.
[29] Fischer-Cripps, A. C. (2002). *Nanoindentation*. New York: Springer-Verlag, p. 53.